Moving Path Following for Autonomous Robotic Vehicles

Tiago Oliveira[1] Pedro Encarnação[2] A. Pedro Aguiar[3]

***Abstract*— This paper introduces the moving path following (MPF) problem for autonomous robotic vehicles, in which the vehicle is required to converge to and follow a desired geometric moving path, without a specific temporal specification. This case generalizes the classical path following problem, where the given path is stationary. Possible tasks that can be formulated as a MPF problem include terrain/air vehicles target tracking and gas clouds monitoring, where the velocity of the target/cloud specifies the motion of the path. Using the concept of parallel-transport frame associated to the geometric path, we derive the MPF kinematic-error dynamics for 3D paths with arbitrary motion specified by its linear and angular velocity. An application is made to the problem of tracking a target on the ground using an Unmanned Aerial Vehicle. The control law is derived using Lyapunov methods. Formal convergence results are provided and hardware in the loop simulations demonstrate the effectiveness of the proposed method.**

I. Introduction

Two typical motion control problems for autonomous robotic vehicles are trajectory tracking and path following. Trajectory tracking (where a vehicle should follow a given trajectory with time constraints) and path following (where there are no time constraints and the vehicle can thus, for example, move with constant speed) control laws for wheeled mobile vehicles have been proposed in a series of groundbreaking papers by Samson et al. (see e.g., [1] and the references therein). For path following a classical approach consists of defining the error space using the Serret-Frenet frame concept [2], or a parallel transport frame [3], [4] associated to the path. The same circle of ideas led to the development of trajectory tracking and path following systems for marine vehicles [5], [6] and unmanned aerial vehicles (UAVs) [4], [7], [8]. Alternative approaches include [9], [10] and [11].

In this paper, we introduce the moving path following (MPF) method to the general case of desired paths moving with time-varying linear and angular velocities, and with non-constant curvature and torsion. It is important to stress that MPF is not trajectory tracking because the path to be followed does not include explicitly time constraints. By further extending the ideas in [12], we provide a generic tool to follow time-varying paths (generalizing the classical path following for stationary paths) that can be applied to different vehicles moving in a 3 dimensional space (e.g., UAVs, AUVs) and mission scenarios, like thermals navigation, gas clouds monitoring or terrain/air vehicles tracking. We derive the MPF kinematic-error dynamics for this general case.

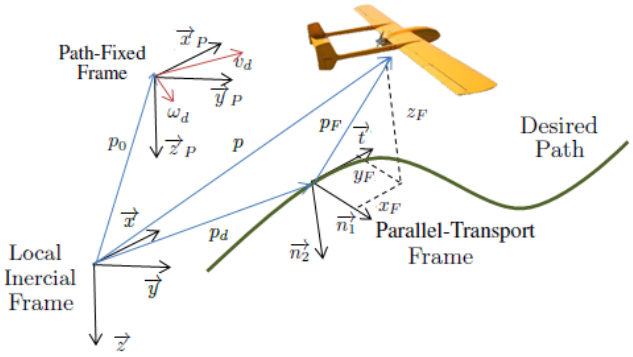

Fig. 1. Error space frames, illustrating for the case of an UAV.

An application example using an UAV is presented, and the control law is derived using Lyapunov methods, assuming that the UAV flies at a constant altitude and airspeed.

The paper is organized as follows. Section II describes the 3D moving path following error space, and then, Section III applies it to the problem of tracking a target on the ground by an UAV. Section IV presents hardware in the loop (HIL) simulations that demonstrate the effectiveness of the proposed method. Finally, Section V presents the main conclusions and future work.

II. Error Space for Moving Path Following

This section presents the MPF problem and formulates the general kinematic model, which is written with respect to the parallel-transport frame (see definition e.g., [3], [4]), associated to the given reference path.

Consider a local inertial frame $\{I\} = \{\overline{x}, \overline{y}, \overline{z}\}$ with the $\overline{x}$ axis pointing North, $\overline{y}$ East and $\overline{z}$ Down (this definition is typically referred to as the North-East-Down (NED) with x-North, y-East, and z-Down). Let $p_d(\ ) = \begin{bmatrix} p_{d_x}(\ ) & p_{d_y}(\ ) & p_{d_z}(\ ) \end{bmatrix}^T$ be the desired path to be followed parametrized by , where for convenience it will be assumed to be the path length. Note that for a fixed 0, $p_d(\ )$ is a path point expressed in the inertial frame. Consider also a path-fixed frame $\{P\} = \{\overline{x}_P, \overline{y}_P, \overline{z}_P\}$ that specifies the desired motion of the path $p_d(\ )$. We denote by p_0 the origin of $\{P\}$ expressed in $\{I\}$ that is fixed to the path (but this does not necessarily means that p_0 $p_d(\ )$ for some

[1] T. Oliveira is with the Portuguese Air Force Academy Research Center, Sintra, 2715-021, Portugal. tmoliveira@academiafa.edu.pt

[2] P. Encarnação is with the Faculty of Engineering of the Catholic University of Portugal, Rio de Mouro, 2635-631, Portugal. pme@fe.lisboa.ucp.pt

[3] A. P. Aguiar is with the Faculty of Engineering, University of Porto (FEUP), Portugal and with the Laboratory of Robotics and Systems in Engineering and Science (LARSyS), Lisbon, Portugal. pedro.aguiar@fe.up.pt

This work was supported in part by projects CONAV/FCT-PT [PTDC/EEACRO/113820/2009], DAEDALUS/FCT-PT [PTDC/EEA-ELC/122203/2010] and PITVANT (funded by the Portuguese MOD).

- see Figure 1), and by $v_d = \begin{bmatrix} v_{d_x} & v_{d_y} & v_{d_z} \end{bmatrix}^T$ and $\omega_d = \begin{bmatrix} \omega_{d_x} & \omega_{d_y} & \omega_{d_z} \end{bmatrix}^T$ the corresponding linear and angular velocities of the path, respectively, also expressed in $\{I\}$.

The MPF problem can be formulated as follows: Given a robotic vehicle and a desired moving path $\mathcal{P}_d = \{p_d(\theta), p_0, v_d, \omega_d\}$, design a control law that steers and keeps the vehicle in the desired path $p_d(\theta)$ with a given speed velocity V.

Let $\{F\} = \{\overline{t}, \overline{n}_1, \overline{n}_2\}$ be the parallel-transport frame associated to the reference path with its orthonormal vectors (see Figure 1) satisfying the frame equations [3],

$$\begin{bmatrix} \frac{d\,\overline{t}}{d} \\ \frac{d\,\overline{n}_1}{d} \\ \frac{d\,\overline{n}_2}{d} \end{bmatrix} = \begin{bmatrix} 0 & k_1(\theta) & k_2(\theta) \\ -k_1(\theta) & 0 & 0 \\ -k_2(\theta) & 0 & 0 \end{bmatrix} \begin{bmatrix} \overline{t} \\ \overline{n}_1 \\ \overline{n}_2 \end{bmatrix},$$

where parameters $k_1(\theta)$ and $k_2(\theta)$ are related to the polar coordinates, and to the path curvature and the path torsion through [3], [13],

$$\kappa(\theta) = \sqrt{k_1(\theta)^2 + k_2(\theta)^2} \tag{1}$$

$$\tau(\theta) = -\frac{d}{d\theta} \arctan\frac{k_2(\theta)}{k_1(\theta)}. \tag{2}$$

The $\{I\}$, $\{F\}$ and $\{P\}$ frames are depicted in Figure 1. Additionally, a wind frame $\{W\} = \{\overline{x}_W, \overline{y}_W, \overline{z}_W\}$ is considered, located at the vehicle center of mass and with its $\overline{x}_W$-axis along the direction of the vehicle velocity vector, the $\overline{y}_W$-axis parallel to the $\overline{x} - \overline{y}$ plane, normal to $\overline{x}_W$, and pointing to the right of an observer that moves in the same direction of the aircraft, and $\overline{z}_W$-axis orthogonal to the previous two (see Figure 2). From this definition, ${}^W v_W$, the linear velocity of $\{W\}$ relative to $\{I\}$ and expressed in $\{W\}$, is given by ${}^W v_W = \begin{bmatrix} V & 0 & 0 \end{bmatrix}^T$, where V denotes the vehicle ground speed.

The vehicle center of mass coordinates are denoted by $p = \begin{bmatrix} x & y & z \end{bmatrix}^T$ when expressed in the inertial frame $\{I\}$ and by $p_F = \begin{bmatrix} x_F & y_F & z_F \end{bmatrix}^T$ when expressed in the parallel-transport frame. The desired angular velocity of the path with respect to the inertial frame $\{I\}$, written in the $\{F\}$ frame, can be computed through

$$\begin{aligned} {}^F\omega_d &= {}^F R_I \, \omega_d \\ &= \begin{bmatrix} {}^F\omega_{d_x} & {}^F\omega_{d_y} & {}^F\omega_{d_z} \end{bmatrix}^T \end{aligned}$$

where ${}^F R_I$ is the rotation matrix from $\{I\}$ to $\{F\}$. According to the parallel-transport frame formulas [4], and admitting that the path is also rotating with an angular velocity given by ${}^F\omega_d$, the angular velocity of the $\{F\}$ frame with respect to the inertial frame, written in the $\{F\}$ frame, is given by

$${}^F\omega_F = \begin{bmatrix} {}^F\omega_{d_x} & -k_2(\theta)\dot{\theta} + {}^F\omega_{d_y} & k_1(\theta)\dot{\theta} + {}^F\omega_{d_z} \end{bmatrix}^T.$$

The linear velocity of $\{W\}$ relative to $\{I\}$ and expressed in $\{I\}$ satisfies

$${}^I v_W = \begin{bmatrix} \dot{x} & \dot{y} & \dot{z} \end{bmatrix}^T = {}^I R_W \, {}^W v_W,$$

where ${}^I R_W$ is the rotation matrix from $\{W\}$ to $\{I\}$.

The position of the UAV in the $\{I\}$ frame can be written as (Figure 1)

$$p = p_d + {}^I R_F \, p_F \tag{3}$$

where ${}^I R_F$ is the rotation matrix from $\{F\}$ to $\{I\}$. Differentiating (3) with respect to time yields

$$\dot{p} = \dot{p}_d + {}^I R_F \, \dot{p}_F + {}^I R_F \, S\left({}^F\omega_F\right) p_F,$$

where $S(.)$ is a skew-symmetric matrix that satisfies $S(a)\, b = a \times b$. Pre-multiplying by ${}^F R_I$ one obtains

$${}^F R_I \dot{p} = {}^F R_I \, \dot{p}_d + \dot{p}_F + S\left({}^F\omega_F\right) p_F. \tag{4}$$

The linear velocity ${}^F R_I \, \dot{p}_d$ of a point on the path relative to $\{I\}$ and expressed in $\{F\}$ is the sum of the linear velocity of the point relative to $\{F\}$ given by ${}^F v_F = \begin{bmatrix} \dot{\theta} & 0 & 0 \end{bmatrix}^T$, with the velocity of the parallel-transport frame relative to $\{I\}$, both expressed in $\{F\}$, i.e.

$${}^F R_I \, \dot{p}_d = {}^F v_F + {}^F R_I \left(v_d + \underbrace{S(p_d - p_0)\,\omega_d}_{v_P} \right), \tag{5}$$

where $(p_d - p_0) = \begin{bmatrix} x & y & z \end{bmatrix}^T$ is the vector from the origin of $\{P\}$ to the origin of the $\{F\}$ frame on the path. The path may rotate around p_0, and thus, v_P is the linear velocity of p_d, due to path's angular velocity. Note that p_0 also moves together with the path ($\dot{p}_0 = v_d$), and thus the relative distance between the center of rotation of the path (p_0) and each path point remains the same. The left side of (4) can be rewritten as,

$${}^F R_I \dot{p} = {}^F R_W \, {}^W v_W. \tag{6}$$

Therefore, combining (5) with (6), equation (4) gives

$$\begin{aligned} \dot{p}_F = {}^F R_W \, {}^W v_W - S\left({}^F\omega_F\right) p_F - {}^F v_F \\ - {}^F R_I \left(v_d + S(p_d - p_0)\,\omega_d \right). \end{aligned} \tag{7}$$

The relative angular velocity between the $\{F\}$ frame and the wind frame $\{W\}$, expressed in $\{W\}$, is given by

$${}^W r_{W,F} = {}^W\omega_W - {}^W\omega_F \tag{8}$$

and thus,

$${}^F\dot{R}_W = {}^F R_W \, S\left({}^W r_{W,F}\right). \tag{9}$$

The complete MPF kinematic error dynamics is given by equations (7) and (9).

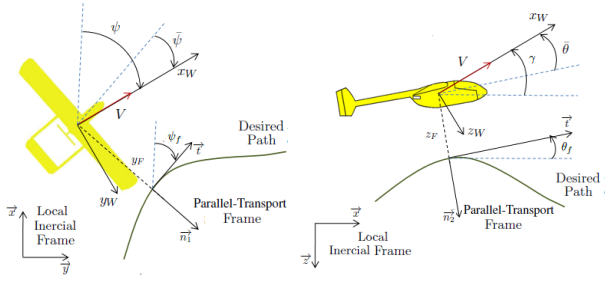

(a) Lateral dynamics (b) Longitudinal dynamics

Fig. 2. Path following relevant variables, illustrating for the case of an UAV.

III. Moving Path following control law: an application to ground target tracking by an UAV

In this section we start by particularizing the error space defined in Section II to the case where Euler angles are used to parametrize the rotation matrices between reference frames, assuming that the flight path angle will always be different from /2. Then, an application is made to ground target tracking by an UAV.

Starting with the path-following controller, the goal is to drive the linear distances x_F, y_F and z_F to zero and orient the UAV such that its velocity vector is aligned with the vector sum of the parallel-transport frame tangent vector and the velocity of the parallel-transport frame origin. Note that by imposing this goal to the kinematic path-following, we encompass the classical situation of following paths that are fixed in space [14], [5], [4].

Let be the angle between the projection of the vehicle velocity vector onto the $\overline{x}-\overline{y}$ plane and North, and let be the angle between the vehicle velocity vector and the $\overline{x}-\overline{y}$ plane, positive if the third component of the velocity vector expressed in $\{I\}$ is negative. Note that these are not regular yaw and pitch angles since they are the angles between the wind frame and the inertial frame instead of the angles between a body frame attached to the vehicle and the inertial frame. Figure 2 shows the error space for path following.

Additionally, let $_f$, $_f$ and $_f$ be the roll, pitch and yaw angles that parametrize the rotation matrix from $\{I\}$ to $\{F\}$. The angular displacements between the wind frame and the parallel-transport frame are $\bar{} = - _f$, $\bar{} = - _f$ and $\bar{} = - _f$ (see Figure 2).

Taking into account the last notation, the UAV kinematic equations expressed in $\{I\}$ are given by

$$\begin{aligned}\dot{x} &= V\cos \cos \\ \dot{y} &= V\cos \sin \\ \dot{z} &= -V\sin \ .\end{aligned}$$

The angular rates $\dot{}$ and $\dot{}$ are related to the angular velocity of the wind frame with respect to the inertial frame, expressed in the wind frame, $^W{}_W = \begin{bmatrix} q_w & r_w \end{bmatrix}^T$ through the Jacobian operator [15] (note that the wind frame roll angle is, by definition, always equal to zero)

$$\begin{bmatrix}\dot{} \\ \dot{}\end{bmatrix} = \begin{bmatrix}1 & 0 \\ 0 & \sec \end{bmatrix}\begin{bmatrix} q_w \\ r_w \end{bmatrix}.$$

The movement of the origin of the $\{P\}$ frame is described by the kinematic equations in terms of the total speed $||v_d||$, the pitch angle $_d$ and the yaw angle $_d$

$$\begin{aligned} v_{d_x} &= ||v_d||\cos \ _d \cos \ _d \\ v_{d_y} &= ||v_d||\cos \ _d \sin \ _d \\ v_{d_z} &= -||v_d||\sin \ _d. \end{aligned}$$

Therefore, equation (7) can be rewritten as

$$\begin{bmatrix}\dot{x}_F \\ \dot{y}_F \\ \dot{z}_F\end{bmatrix} = \begin{bmatrix} V\cos\bar{\theta}\cos\bar{\psi} \\ V\cos\bar{\theta}\sin\bar{\psi} \\ -V\sin\bar{\theta}\end{bmatrix} - \begin{bmatrix}0 \\ 0 \\ 0\end{bmatrix} - {}^F R_I(\phi_f,\theta_f,\psi_f)\begin{bmatrix} v_{d_x} \\ v_{d_y} \\ v_{d_z}\end{bmatrix} + \begin{bmatrix} \omega_{d_x} \\ \omega_{d_y} \\ \omega_{d_z}\end{bmatrix} \times \begin{bmatrix} x \\ y \\ z\end{bmatrix}$$

$$= \begin{bmatrix} -\dot{}(k_1(\) y_F + k_2(\) z_F) - {}^F\omega_{d_z} y_F + {}^F\omega_{d_y} z_F \\ -\begin{bmatrix} x_F k_1\dot{} + {}^F\omega_{d_z}\end{bmatrix} - {}^F\omega_{d_x} z_F \\ x_F k_2\dot{} - {}^F\omega_{d_y} + {}^F\omega_{d_x} y_F\end{bmatrix}.$$

The relative angular velocity between $\{F\}$ and the wind frame $\{W\}$, expressed in $\{W\}$, as given by equation (8) can now be written as

$$\begin{bmatrix}\bar{p} \\ \bar{q} \\ \bar{r}\end{bmatrix} = \begin{bmatrix}0 \\ q_w \\ r_w\end{bmatrix} - {}^W{}_F \tag{10}$$

where

$${}^W\omega_F = {}^W R_F(\bar{\phi},\bar{\theta},\bar{\psi})\,{}^F\omega_F$$

$$= {}^W R_F(\bar{\phi},\bar{\theta},\bar{\psi})\begin{bmatrix} {}^F\omega_{d_x} \\ -k_2(\)\dot{} + {}^F\omega_{d_y} \\ k_1(\)\dot{} + {}^F\omega_{d_z}\end{bmatrix}.$$

Using the Jacobian operator that relates the roll, pitch and yaw angle rates with the angular velocities [15], one can rewrite equation (9) as

$$\begin{bmatrix}\dot{} \\ \dot{} \\ \dot{}\end{bmatrix} = \begin{bmatrix}1 & \sin\bar{}\tan\bar{} & \cos\bar{}\tan\bar{} \\ 0 & \cos\bar{} & -\sin\bar{} \\ 0 & \frac{\sin\bar{}}{\cos} & \frac{\cos\bar{}}{\cos}\end{bmatrix}\begin{bmatrix}\bar{p} \\ \bar{q} \\ \bar{r}\end{bmatrix}.$$

The roll rate equation can be omitted since errors in roll between $\{W\}$ and $\{F\}$ do not affect convergence to the path (in practice, the vehicle will assume a roll angle that enables it to follow the path). Solving (10) with respect to the pitch and yaw angle rates gives

$$\begin{bmatrix}\dot{} \\ \dot{}\end{bmatrix} = D(\bar{},\bar{}) + T(\bar{},\bar{})\begin{bmatrix} q_w \\ r_w\end{bmatrix}$$

with

$$D(\bar{\theta},\bar{\psi}) = \begin{bmatrix} \dot{}\cos\bar{\psi}\,k_2(\) - \cos\bar{\psi}\,{}^F\omega_{d_y} \\ -\dot{}k_1(\) - {}^F\omega_{d_z} - \tan\bar{\theta}\sin\bar{\psi}\,\dot{} - k_2(\) + {}^F\omega_{d_y}\end{bmatrix}$$

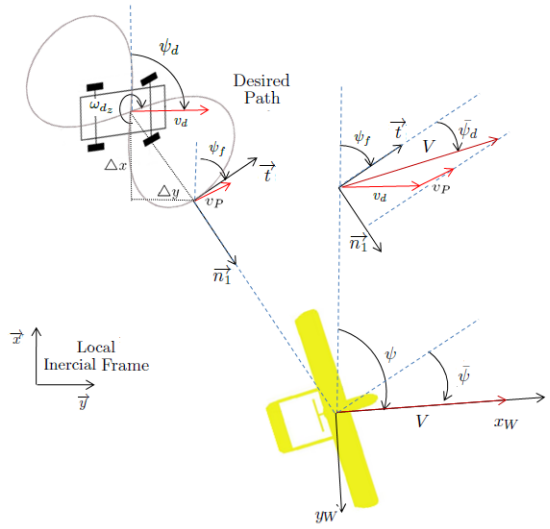

Fig. 3. Moving path following: relevant variables.

and

$$T\ ^{-},^{-} = \begin{matrix} \cos\ ^{-} & -\sin\ ^{-} \\ \frac{\sin\ ^{-}}{\cos} & \frac{\cos\ ^{-}}{\cos} \end{matrix}.$$

Using the feedback linearization law

$$\begin{matrix} q_w \\ r_w \end{matrix} = T^{-1}\ ^{-},^{-} \begin{matrix} u \\ u \end{matrix} - D\ ^{-},^{-}$$

one can write

$$\begin{matrix} \dot{} & = & u \\ \dot{} & = & u \end{matrix}$$

where u and u are the new control input signals.

As an application example, the problem of tracking a target on the ground by an UAV is considered. A lemniscate has been shown to be an effective way for an autonomous aircraft to provide surveillance of a slower target [16]. The proposed strategy is thus to follow a lemniscate path centered at the actual target position whose angular velocity is the same as the target, keeping the UAV altitude constant (Figure 3). For this application, the origin of the parallel-transport frame is always placed at the point on the path that is closest to the vehicle. The ground target tracking control law derived here is an extension of the strategy presented in [12].

From equations (1) and (2) it can be shown that for a planar path, the corresponding parallel-transport frame $k_1(\ )$ and $k_2(\ )$ parameters are

$$\begin{aligned} k_1(\ ) &= \ (\ ) \\ k_2(\ ) &= 0 \end{aligned}$$

Thus, for this application, $x_F = \dot{x}_F = z_F = \dot{z}_F = \ _f = \ _ = \ _ = \ = \ _{d_x} = \ _{d_y} = 0$ and the error space can be simplified to yield, assuming $1 - \ (\ )\, y_F = 0$

$$\begin{aligned} \dot{\square} &= \frac{\mathsf{V}\ \cos\bar{\psi} - (\mathsf{v}_{d_x} - \omega_{d_z}\square\,\mathsf{y})\cos\psi_f}{1 - \kappa(\square)\,\mathsf{y}_F} \\ &\quad - \frac{\mathsf{v}_{d_y} + \omega_{d_z}\square\,\mathsf{x}\ \ \sin\psi_f - \omega_{d_z}\,\mathsf{y}_F}{1 - \kappa(\square)\,\mathsf{y}_F} \\ \dot{\mathsf{y}}_F &= \mathsf{V}\ \sin\bar{\psi} + (\mathsf{v}_{d_x} - \omega_{d_z}\square\,\mathsf{y})\sin\psi_f - \ \square\ \mathsf{v}_{d_y} + \omega_{d_z}\square\,\mathsf{x}\ \ \cos\psi_f \\ \dot{\bar{\psi}} &= \mathsf{u}_\psi . \end{aligned} \tag{11}$$

The steady state value $\ _d$ for can be computed from (11) by setting $\dot{y}_F = 0$, which yields

$$\bar{\psi}_\mathsf{d} = \arcsin\square\ \frac{-\ (\mathsf{v}_{d_x} - \omega_{d_z}\square\,\mathsf{y})\sin\psi_f + \ \square\ \mathsf{v}_{d_y} + \omega_{d_z}\square\,\mathsf{x}\ \ \cos\psi_f}{\mathsf{V}}\square$$

Note that the numerator of the arcsin argument is the sum of target's speed (v_d) with the linear velocity of the origin of $\{F\}$, v_P, along the normal to the path. This means that the above equation is always well defined if the UAV speed V is greater than the sum of the target speed, v_d , with the parallel-transport frame speed, v_P , and thus the path following problem is well posed.

In order to avoid situations in which the UAV is required to fly near its stall speed, it is desirable to keep the vehicle airspeed (denoted by V_0) constant. Commercial autopilots usually accept airspeed references, expressed in the vehicle body frame. The vehicle velocity relative to $\{I\}$ and expressed in the wind frame $\{W\}$, is given by

$${}^W v_W = {}^W R_B(\ ,\ )\, V_0 + {}^W R_I(\ ,\ )\, {}^I v_{wind}$$

where ${}^I v_{wind}$ denotes the velocity of the wind relative to $\{I\}$ and expressed in $\{I\}$ and ${}^W R_B$ is a rotation matrix parameterized by the vehicle angle of attack and the sideslip angle [17]. In general, for fixed wing UAVs, these angles are usually small, and therefore it is reasonable to assume that ${}^W R_B = I$. With this assumption (and since $= 0$ for planar reference paths), one can write the UAV's ground speed as

$$V = V_0 + W_t,$$

where W_t is the tangential component of the wind pointing in the same direction as the velocity vector of the aircraft, being given by

$$W_t = w_x \cos\ \ + w_y \sin\ .$$

The derivative of $\ _d$ with respect to time, that will be necessary in the sequence, assuming that the autopilot is able to keep V_0 constant, is

$$\begin{aligned} \dot{\bar{\psi}}_\mathsf{d} &= \square\ \frac{\rho}{\mathsf{V}\ \ 1 - \frac{-(\mathsf{v}_{d_x} - \omega_{d_z}\square\,\mathsf{y})\sin\psi_f + (\mathsf{v}_{d_y} + \omega_{d_z}\square\,\mathsf{x})\cos\psi_f}{\mathsf{V}}\square^2} \\ &\quad - \dot{\psi}\ \square\ \frac{\lambda}{\mathsf{V}^2\ \ 1 - \frac{-(\mathsf{v}_{d_x} - \omega_{d_z}\square\,\mathsf{y})\sin\psi_f + (\mathsf{v}_{d_y} + \omega_{d_z}\square\,\mathsf{x})\cos\psi_f}{\mathsf{V}}\square^2} \end{aligned} \tag{12}$$

where

$$\rho = -\dot{\psi}_f \left(v_{d_x} - \omega_{d_z} y\right) + \dot{\omega}_{d_z} x + \omega_{d_z} \dot{x} \cos\psi_f + -\dot{\psi}_f \; v_{d_y} + \omega_{d_z} x + \dot{\omega}_{d_z} y + \omega_{d_z} \dot{y} \sin\psi_f + \|v_d\| \dot{\psi}_d \cos(\psi_d - \psi_f) + \dot{v}_d \sin(\psi_d - \psi_f)$$

$$\lambda = (-w_x \sin\psi + w_y \cos\psi) \left(-\left(v_{d_x} - \omega_{d_z} y\right) \sin\psi_f + v_{d_y} + \omega_{d_z} x \cos\psi_f\right),$$

with

$$\dot{x} = \cos \; _f - \; _{d_z} \; y$$
$$\dot{y} = \sin \; _f + \; _{d_z} \; x.$$

Equation (12) can be cast in the compact form

$$\dot{} \; _d = P - \; ^{\cdot} \quad ,$$

with

$$P = \frac{}{V \quad 1 - \frac{-\left(v_{d_x} - \; _{d_z} y\right) \sin \; _f + \left(v_{d_y} + \; _{d_z} x\right) \cos \; _f}{V}^2}$$

and

$$= \frac{}{V^2 \quad 1 - \frac{-\left(v_{d_x} - \; _{d_z} y\right) \sin \; _f + \left(v_{d_y} + \; _{d_z} x\right) \cos \; _f}{V}^2}.$$

To derive a control law for moving path following, consider now the Lyapunov function

$$V_1 = \frac{1}{2} \quad y_F^2 + \frac{1}{g_2} \; ^{\tilde{}2} \quad , \tag{13}$$

where $^{\tilde{}} = \; ^{-} - \; ^{-}_d$ and $g_2 > 0$.

***Theorem* 1**

Considering the control law

$$\dot{} = (-g_1 \; ^{\tilde{}} + \quad (\;)^{\cdot} + \; _{d_z} + P - g_2 \, y_F (((v_{d_x} - \; _{d_z} \quad y) \sin \; _f - \; v_{d_y} + \; _{d_z} \quad x \quad \cos \; _f)) \frac{1 - \cos \; ^{\tilde{}}}{\tilde{}} + V \cos \; _d \frac{\sin \; ^{\tilde{}}}{\tilde{}}))/(1 + \quad) \tag{14}$$

then the closed loop error signals $^{\tilde{}}$ and y_F converge to zero as t .

Theorem 1 can be deduced from standard Lyapunov arguments using the Lyapunov function (13) and the Barbalat lemma [18].

The $\dot{}$ control law (14) is converted to a bank reference for the inner-loop controller through the coordinated turn relation [4].

Controller Parameters

g_1	=	0.22	ω_{d_z}	=	$\dot{\psi}_d$
g_2	=	0.0007	$\dot{\omega}_{d_z}$	=	$\ddot{\psi}_d = -0.0006\sin(0.03\,t)$

TABLE I

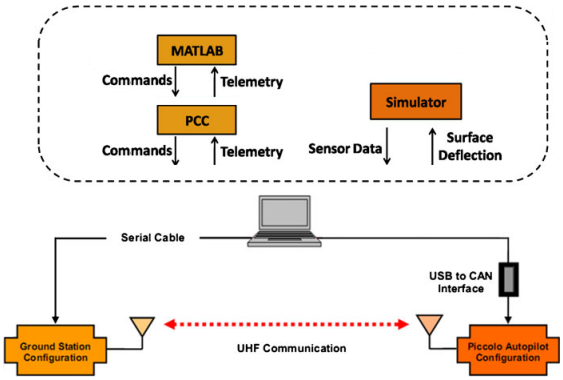

Fig. 4. Control system architecture used in the HIL simulations. Adapted from Piccolo Setup Guide [20]

IV. Simulation Results

The proposed control law was tested through hardware in the loop (HIL) simulations, using the ANTEX-X02 aircraft model within the test bed reported in [19]. The UAV has an off-the-shelf inner loop controller that accepts references at kinematic level (angular rates and linear velocities) and generates the UAV control signals necessary to follow those references in the presence of model uncertainty and external disturbances, like wind. The outer loop control laws derived in the previous section provides the references to the inner control loop.

In the simulation results here presented, the UAV was required to track a target by following a lemniscate with a 200m distance between foci, keeping the line that connects the two foci always perpendicular to $_d$, moving together with the target, at 20m/s airspeed.

The target was moving according to

$$(p_{d_x},\, p_{d_y}, \quad _d,\, v_d)|_{t=0} = (0\text{m},\ 0\text{m},\ 0,\ 4\text{m/s})$$
$$\dot{v}_d = 0.2\sin(0.07\,t)$$
$$\dot{} \; _d = 0.02\cos(0.03\,t)$$

where t corresponds to the simulation time. The controller parameters used are listed in Table I.

The hardware in the loop simulations were done using a laptop that simultaneously ran the control algorithm and the simulated aircraft dynamics (see Figure 4). Via its RS-232 port, the laptop received the sensors data from the Piccolo autopilot [20] and provided to the Piccolo the control references; through a CAN bus, the laptop received the control surface and thrust signals from the Piccolo and returned the corresponding sensors data to the Piccolo. The telemetry signals from the aircraft were synchronized with a "faked" GPS data of the target at 1Hz and then fed to the controller to compute the bank reference to the aircraft.

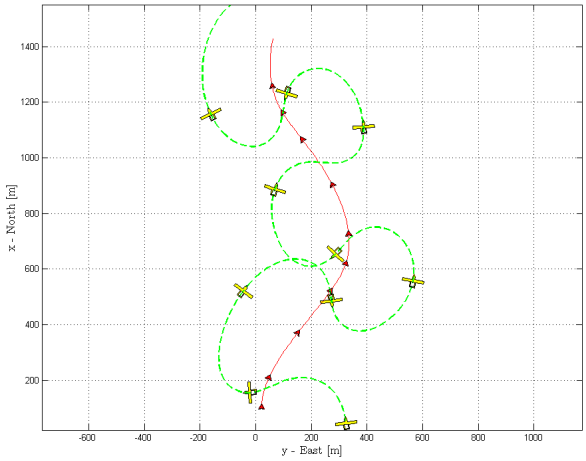

Fig. 5. Aircraft's trajectory following a target.

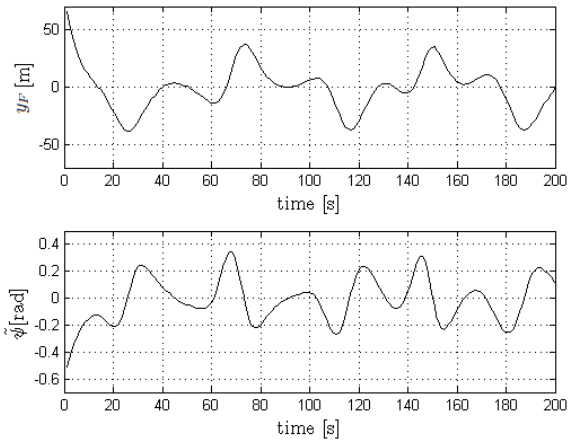

Fig. 6. Position and heading errors.

Figures 5 - 7 shows HIL simulation results which demonstrate the performance of the overall control system. The control surface deflections are kept within their linear regions. Figure 7 shows that there is a considerable delay between the reference bank and its actual value.

V. Conclusions

An error space for moving path following was presented, by formally extending the classic path following algorithms to the case of time varying paths in a three dimensional space. The error space derived was used to design a kinematic ground target tracking control law for UAVs equipped with an autopilot that accepts references at the kinematic level. HIL simulation results demonstrates the effectiveness of the proposed method. Future work will include the flight test of the control law onboard the aircraft and address the problem of acquiring target's position and velocity using passive sensors.

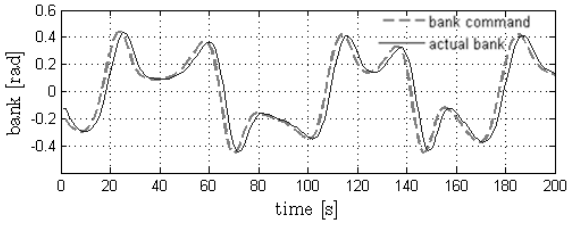

Fig. 7. Bank reference command and real value.

References

[1] C. Wit, H. Khennouf, C. Samson, and O. Sordalen, "Nonlinear control design for mobile robots," Recent Trends in Mobile Robots, vol. 11, pp. 121–156, 1993.

[2] I. Kaminer, O. Yakimenko, A. Pascoal, and R. Ghabcheloo, "Path generation, path following and coordinated control for time-critical missions of multiple UAVs," in Proceedings of the 2006 American Control Conference, 2006, pp. 4906–4913.

[3] L. Bishop, "There is more than one way to frame a curve," in Amer. Math. Monthly 82, March 1975, pp. 246 – 251.

[4] I. Kaminer, A. Pascoal, C. Cao, and V. Dobrokhodov, "Path following for unmanned aerial vehicles using L1 adaptive augmentation of commercial autopilots," Journal of Guidance, Control and Dynamics, vol. 33, pp. 550 – 564, 2010.

[5] P. Encarnação and A. Pascoal, "3D path following for autonomous underwater vehicles," in Proceedings of the 39th Conference on Decision and Control, 2000, pp. 2977 – 2982.

[6] L. Lapierre, D. Soetanto, and A. Pascoal, "Adaptive, non-singular path-following control of dynamic wheeled robots," in Proceedings of the 42nd IEEE Conference on Decision and Control, vol. 2, 2003, pp. 1765–1770.

[7] E. Frew, D. Lawrence, C. Dixon, J. Elston, and J. Pisano, "Lyapunov guidance vector fields for unmanned aircraft applications," in Proceedings of the 2007 American Control Conference, 2007, pp. 371 – 376.

[8] R. Wise and R. Rysdyk, "UAV coordination for autonomous target tracking," in Proceedings of the AIAA Guidance, Navigation, and Control Conference and Exhibit, 2006.

[9] J. Hauser and R. Hindman, "Aggressive flight maneuvers," in Proceedings of the 36th Conference on Decision and Control, 1997, pp. 4186–4191.

[10] R. Skjetne, T. Fossen, and P. Kokotović, "Robust output maneuvering for a class of nonlinear systems," Automatica, vol. 40, pp. 373–383, 2004.

[11] A. Aguiar and J. Hespanha, "Trajectory-tracking and path-following of underactuated autonomous vehicles with parametric modeling uncertainty," IEEE Transactions on Automatica Control, vol. 52, pp. 1362 – 1379, 2007.

[12] T. Oliveira and P. Encarnação, "Ground target tracking control system for unmanned aerial vehicles," Journal of Intelligent and Robotic Systems, vol. 69, pp. 373 – 387, 2013.

[13] A. Hanson and H. Ma, "Parallel transport approach to curve framing," Indiana University, Tech. Rep., 1995.

[14] C. Samson, "Path following and time-varying feedback stabilization of wheeled mobile robots," in Proceedings of the International Conference on Advanced Robotics and Computer Vision, vol. 13, 1992.

[15] B. Siciliano, L. Sciavicco, L. Villani, and G. Oriolo, Robotics: Modelling, Planning and Control, S. London, Ed. Springer, 2011.

[16] S. Spry, A. Vaughn, and X. Xiao, "A vehicle following methodology for UAV formations," in Proceedings of the 4th International Conference on Cooperative Control and Optimization, 2003.

[17] A. Aguiar, I. Kaminer, R. Ghabcheloo, A. Pascoal, E. Xargay, N. Hovakimyan, C. Cao, and V. Dobrokhodov, "Time-coordinated path following of multiple UAVs over time-varying networks using L1 adaptation," in Proceedings of the AIAA Guidance, Navigation and Control Conference and Exhibit, 2008.

[18] H. Khalil, Nonlinear Systems, Prentice Hall ed., 2002.

[19] T. Oliveira, G. Cruz, E. Marques, and P. Encarnação, "A test bed for rapid flight testing of UAV control algorithms," in Proceedings of RED-UAS 2011 - Research, Development and Education on Unmanned Aerial Systems, 2011.

[20] Vaglienti, Hoag, Niculescu, Becker, and Miley, Piccolo System User's Guide, Cloud Cap Technology, 2009.